

SLC46A3 is a lysosomal proton-coupled steroid conjugate and bile acid transporter involved in transport of active catabolites of T-DM1

Ryuto Tomabechi^a, Hisanao Kishimoto^a, Taeka Sato^a, Naoki Saito^a, Keisuke Kiyomiya^a, Tappei Takada^b, Kei Higuchi^a, Yoshiyuki Shirasaka^c and Katsuhisa Inoue^{a,*}

^aDepartment of Biopharmaceutics, School of Pharmacy, Tokyo University of Pharmacy and Life Sciences, 1432-1, Horinouchi, Hachioji, Tokyo 192-0392, Japan

^bDepartment of Pharmacy, The University of Tokyo Hospital, 7-3-1 Hongo, Bunkyo-ku, Tokyo 113-8655, Japan

^cFaculty of Pharmacy, Institute of Medical, Pharmaceutical and Health Sciences, Kanazawa University, Kakuma-machi, Kanazawa 920-1192, Japan

*To whom correspondence should be addressed: Email: kinoue@toyaku.ac.jp

Edited By: Karen E. Nelson.

Abstract

Antibody–drug conjugates (ADCs) represent a new class of cancer therapeutics that enable targeted delivery of cytotoxic drugs to cancer cells. Although clinical efficacy has been demonstrated for ADC therapies, resistance to these conjugates may occur. Recently, SLC46A3, a lysosomal membrane protein, was revealed to regulate the efficacy of trastuzumab emtansine (T-DM1), a noncleavable ADC that has been widely used for treating breast cancer. However, the role of SLC46A3 in mediating T-DM1 cytotoxicity remains unclear. In this study, we discovered the function of SLC46A3 as a novel proton-coupled steroid conjugate and bile acid transporter. SLC46A3 preferentially recognized lipophilic steroid conjugates and bile acids as endogenous substrates. In addition, we found that SLC46A3 directly transports Lys-SMCC-DM1, a major catabolite of T-DM1, and potent SLC46A3 inhibitors attenuate the cytotoxic effects of T-DM1, suggesting a role in the escape of Lys-SMCC-DM1 from the lysosome into the cytoplasm. Our findings reveal the molecular mechanism by which T-DM1 kills cancer cells and may contribute to the rational development of ADCs that target SLC46A3.

Keywords: antibody–drug conjugate, bile acid, SLC46A3, steroid conjugate, and trastuzumab emtansine

Significance Statement:

Trastuzumab emtansine (T-DM1) is an antibody–drug conjugate that has been used for the treatment of HER2-positive breast cancer. Previous studies have shown that SLC46A3, a lysosomal membrane protein, is associated with T-DM1 cytotoxicity and clinical efficiency. However, the mechanism by which SLC46A3 is involved in T-DM1 cytotoxicity remains unclear. In this study, we discovered that SLC46A3 functions as a proton-driven transporter for steroid conjugates and bile acids as well as for Lys-SMCC-DM1, an active catabolite of T-DM1. Furthermore, we demonstrated that the cytotoxic effects of T-DM1 were significantly reduced in the presence of SLC46A3 inhibitors identified in this study. Our findings established that SLC46A3 is involved in the lysosomal escape of Lys-SMCC-DM1 into the cytoplasm leading to anticancer efficacy.

Introduction

Antibody–drug conjugates (ADCs) represent a new class of cancer therapeutics that deliver cytotoxic agents specifically to tumors (1, 2). An ADC consists of a monoclonal antibody, cytotoxic drug (payload), and linkers to conjugate the antibody and payload. This results in damage specifically to cancer cells expressing the target antigen of the antibody, thereby reducing off-target cytotoxic effects. Currently, there are 11 ADCs approved by the Food and Drug Administration (FDA) and a considerable number in clinical trials (3, 4).

ADCs induce a pharmacological effect through a multistep process which includes binding to the cell surface antigen, internalization into endosomes/lysosomes, catabolism to release the payload, and escape from lysosomes (1). Although internalization is a

common rate-limiting step for payload release from ADCs, additional steps may occur depending on whether the linker types are cleavable or noncleavable (5). The ADCs conjugated with cleavable linkers are decomposed in the endosomes or lysosomes after internalization to yield the payload, which is generally highly membrane permeable and readily diffuses from lysosomes into the cytoplasm. In contrast, those with noncleavable linkers are not cleaved, producing a linker-bound payload, which is a high molecular weight complex and comparably hydrophilic because of the conjugated amino acid residue at the terminus (6, 7). Hence, the linker-bound payload is considered impermeable and requires carriers, such as transporters, to be released from the lysosomes.

Trastuzumab emtansine (T-DM1) is a successful noncleavable ADC that has been widely used in clinical practice for the

Competing interest: The authors declare no potential conflicts of interest.

Received: February 2, 2022. **Accepted:** May 17, 2022

© The Author(s) 2022. Published by Oxford University Press on behalf of the National Academy of Sciences. This is an Open Access article distributed under the terms of the Creative Commons Attribution-NonCommercial-NoDerivs licence (<https://creativecommons.org/licenses/by-nc-nd/4.0/>), which permits non-commercial reproduction and distribution of the work, in any medium, provided the original work is not altered or transformed in any way, and that the work is properly cited. For commercial re-use, please contact journals.permissions@oup.com

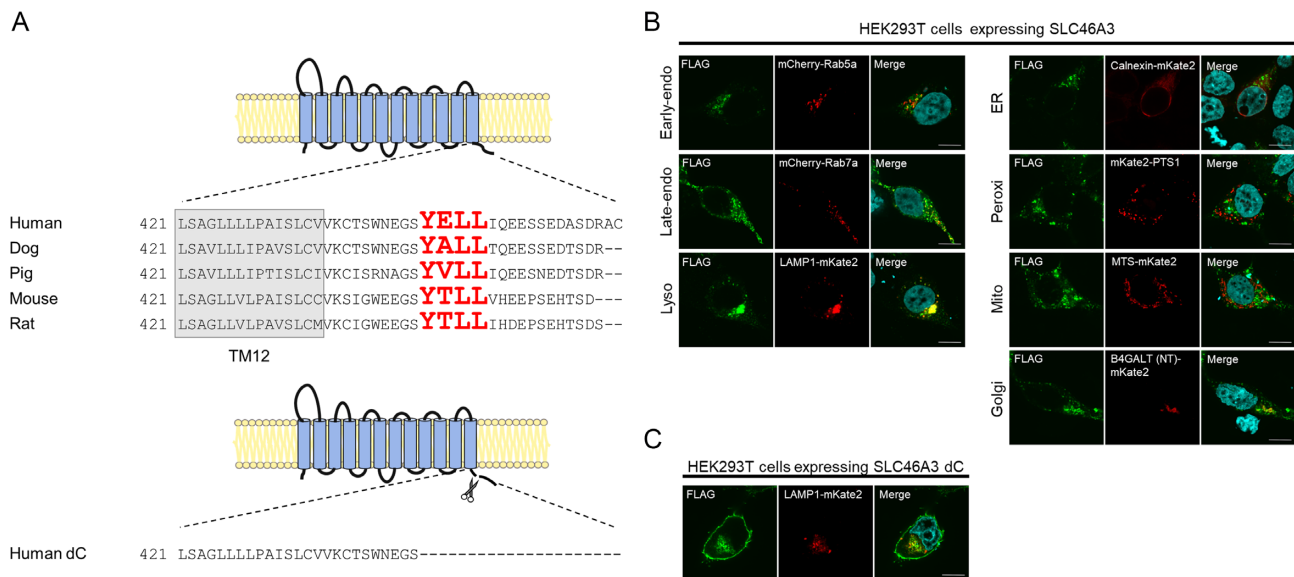


Fig. 1. Mammalian SLC46A3 shares a lysosomal-sorting motif in its C-terminal region. (A) Predicted membrane topology of SLC46A3 by TMHMM (<http://www.cbs.dtu.dk/services/TMHMM/>) and sequence alignment of its C-terminal region between mammalian species. The sequences predicted as tyrosine-based lysosomal-sorting motifs are shown with red color characters. Human dC is a C-terminal amino acid sequence deleted in SLC46A3 mutants in this study. (B) and (C) Immunofluorescence staining of FLAG-tagged SLC46A3 (green) in transfected cells by anti-FLAG antibody. HEK293T cells were transfected with 3 × FLAG-tagged wild-type human SLC46A3 (B) or C-terminal deleted mutant human SLC46A3 (SLC46A3 dC) (C) and mCherry or mKate2-tagged organelle marker protein (red). The results were replicated in three independent experiments. Blue color, nucleus. Scale bar, 10 μ m. PTS1, peroxisomal targeting signal 1; MTS, mitochondrial targeting sequence; and B4GALT (NT), N-terminal 81-amino acid human beta-1,4-galactosyltransferase.

treatment of human epidermal growth factor receptor type 2 (HER2)-positive metastatic breast cancer (8, 9). T-DM1 consists of a monoclonal antibody for HER2, a noncleavable thioether linker, N-succinimidyl 4-(N-maleimidomethyl) cyclohexane-1-carboxylate (SMCC), and N^2 -deacetyl- N^2 -(3-mercapto-1-oxopropyl)-maytansine (DM1), a tubulin inhibitor, which is mainly catabolized to lysine- N^{ϵ} -N-succinimidyl 4-(N-maleimidomethyl) cyclohexane-1-carboxylate-DM1 (Lys-SMCC-DM1) in lysosomes. A previous study using an shRNA screen identified SLC46A3, a lysosomal membrane protein (10), that regulates the lysosomal levels and efficacy of Lys-SMCC-DM1 (11). Recently, it was reported that SLC46A3 expression is associated with T-DM1 resistance and implicated as a prognostic biomarker for patients (12–14). These findings support the importance of SLC46A3 in T-DM1 treatment.

SLC46A3 is an orphan transporter that belongs to the SLC46A family, which includes a well-characterized protein, proton-coupled folate transporter (PCFT also known as SLC46A1) (11, 15). Given its significant similarity with PCFT based on amino acid sequence and membrane topology, SLC46A3 likely functions as a membrane transporter that mediates the transport of solute molecules across the membrane. However, the molecular function of SLC46A3 as a solute transporter and its physiological substrates are unknown.

In this study, we identified SLC46A3 substrates with a functional screening using cells expressing a SLC46A3 mutant that primarily localizes to the plasma membrane. We found that SLC46A3 is a proton-coupled, steroid conjugate, and bile acid transporter. Furthermore, we demonstrated that SLC46A3 transports Lys-SMCC-DM1 and DM1. Our findings reveal a molecular mechanism by which T-DM1 induces its cytotoxicity after degradation in lysosomes and contribute to the understanding of the intracellular dynamics of T-DM1.

Results

SLC46A3 has a tyrosine-based lysosomal-sorting motif at its C-terminus

Lysosomal proteins often contain lysosomal-sorting signals, such as a tyrosine motif or a dileucine motif (16), which are involved in lysosomal localization. To identify whether SLC46A3 contains these signals, we analyzed the primary structure of mammalian SLC46A3 using the ClustalW program (<https://www.genome.jp/tools-bin/clustalw>). We found the amino acid sequence, YELL (Y446–L449), corresponding to a tyrosine-based motif $Yxx\Phi$ (where Φ is hydrophobic residue) in the C-terminal region of human SLC46A3. Similar sequences were identified in other species, suggesting conservation of this sorting signal function among mammals (Fig. 1A).

To confirm the subcellular localization of SLC46A3, we performed immunofluorescence staining with several intracellular organelle markers in HEK293T cells expressing FLAG-tagged SLC46A3 (Fig. 1B). Immunofluorescence staining showed that SLC46A3 was colocalized with LAMP1-mKate2 (lysosomal marker) and partially with mCherry-Rab5a (early-endosomal marker), mCherry-Rab7a (late-endosomal marker), and B4GALT (NT)-mKate2 (Golgi marker). In contrast, SLC46A3 was almost completely unmerged with markers of other compartments, such as calnexin-mKate2 (ER marker), mKate2-PTS1 (peroxisomal marker), and MTS-mKate2 (mitochondrial marker). These results indicate that SLC46A3 mainly localizes to lysosomes.

Next, to localize SLC46A3 to the plasma membrane, we designed a human SLC46A3 mutant (SLC46A3 dC), which is devoid of the C-terminal domain, including YELL (Fig. 1A). Immunofluorescence staining showed that SLC46A3 dC in HEK293T cells localized to the plasma membrane with a proportion of SLC46A3 dC in the intracellular compartment (Fig. 1C). This proportion of

intracellular SLC46A3 dC was merged with Rab7a and LAMP1, suggesting that other endosomal/lysosomal sorting motifs are present in the sequences of SLC46A3 dC (Fig. 1C; Figure S1A, Supplementary Material).

For subsequent studies, we generated a stable cell line expressing SLC46A3 dC using Madin–Darby canine kidney II (MDCKII) cells, which are commonly used for drug transport studies because of a low uptake phenotype by endogenous transporters (17). We confirmed the plasma membrane localization of SLC46A3 dC in MDCKII cells by immunofluorescence staining (Figure S1B, Supplementary Material).

SLC46A3 mediates estrone 3-sulfate transport in a proton-dependent manner

SLC46A3 is a member of the SLC46A family and shares approximately 30% homology of amino acids sequence with SLC46A1, which mediates folate and antifolate drug transport in a proton-dependent manner (18, 19). Therefore, we hypothesized that SLC46A3 transports organic anions under acidic conditions. To test this hypothesis, we performed uptake experiments with organic anions using stable SLC46A3 dC-expressing MDCKII cells (MDCKII/SLC46A3 dC cells). The cells and mock cells were incubated in Hank's Balanced Salt Solution (HBSS) at pH 5.5 for 5 min in the presence of [³H]estrone 3-sulfate, methotrexate, [³H]nicotinate, [³H]palmitate, and [¹⁴C]urate, respectively. The results indicated that estrone 3-sulfate markedly accumulated in MDCKII/SLC46A3 dC cells, and the uptake amount was approximately 10-fold higher compared with mock-transfected cells (Fig. 2A). Furthermore, to validate estrone 3-sulfate uptake by SLC46A3 dC, we conducted the experiment using HEK293T cells transiently expressing FLAG-tagged wild-type SLC46A3 or SLC46A3 dC (Figure S2, Supplementary Material), resulting in a significant uptake of estrone 3-sulfate. These results indicate that SLC46A3 is a transporter that mediates estrone 3-sulfate transport.

To determine whether transport activity is pH-sensitive, we conducted a pH-dependent uptake experiment. As shown in Fig. 2B, the uptake of estrone 3-sulfate in MDCKII/SLC46A3 dC cells was markedly increased with a decline of extracellular pH, reaching a maximum between pH 4.0 and 4.5. At pH 7.4, transport activity dissipated. These results suggest an optimal transport function of SLC46A3 in the lysosomes, where the pH is maintained in a range from 4.5 to 5.0 (20).

Next, we investigated the driving force behind SLC46A3 dC-mediated uptake using nigericin, an ionophore that exchanges K⁺ and H⁺ across the plasma membrane, resulting in dissipation of a proton gradient (19). MDCKII/SLC46A3 dC cells were preincubated with HBSS-modified buffer, in which NaCl was replaced with KCl, containing nigericin prior to incubation with estrone 3-sulfate at pH 5.0 (Fig. 2C). The uptake was significantly decreased in K⁺ buffer with nigericin (condition without a proton gradient), although replacement of NaCl with KCl in the uptake buffer alone (condition to depolarize the membrane potential) did not affect estrone 3-sulfate uptake. Furthermore, substitution of extracellular Na⁺ with *N*-methyl-D-glucamine did not affect the uptake (Figure S3, Supplementary Material). Similarly, uptake was not altered when extracellular Cl⁻ was replaced by gluconate or when Ca²⁺ and Mg²⁺ were removed. These results indicate that SLC46A3 dC mediates the uptake of estrone 3-sulfate using an inward proton gradient as the driving force and suggests that native SLC46A3 mediates an outward directed transport based on a proton gradient across the lysosomal membrane. Finally, to

characterize the kinetic parameters of SLC46A3 dC-mediated estrone 3-sulfate uptake, we performed concentration-dependent uptake experiments and calculated the K_m value based on the Michaelis–Menten equation. As the accumulation of estrone 3-sulfate was elevated up to 5 min and reaching a plateau, the uptake was measured at 1 min (Figure S4, Supplementary Material). The uptake of estrone 3-sulfate mediated by SLC46A3 dC was saturable with a K_m value of 33.3 μ M and a V_{max} of 1.46 nmol/min/mg protein (Fig. 2D and Table 1).

Steroid conjugates and bile acids inhibit SLC46A3 dC-mediated estrone 3-sulfate transport

To investigate the substrate specificity of SLC46A3 dC, we assessed the inhibitory effect of various endogenous compounds on estrone 3-sulfate uptake in MDCKII/SLC46A3 dC cells (Fig. 3). We found that endogenous steroid conjugates, such as sulfate conjugates of dehydroepiandrosterone, pregnenolone, and 25-hydroxyvitamin D₃, and glucuronides of estradiol and 25-hydroxyvitamin D₃, as well as bile acids (cholate, glycocholate, and taurocholate) strongly inhibited estrone 3-sulfate transport mediated by SLC46A3, with the exception of cholesterol sulfate. The deconjugated steroids, however, showed a slight or no significant inhibition of uptake, except for dehydroepiandrosterone, which showed modest inhibition. Glucuronides with a relatively low molecular weight, such as *p*-acetamidophenyl β -D-glucuronide, 4-methylumbelliferyl- β -D-glucuronide, and α -naphthyl β -D-glucuronide, did not decrease the uptake (Figure S5, Supplementary Material). Inhibition by water-soluble vitamins including folates, which are endogenous substrates of SLC46A1 (18, 19), was minimal. Other endogenous organic anions, such as hemin, bilirubin, and ketoglutarate, did not inhibit uptake. Recently, Kim et al. reported that *Slc46a3* knockout mice exhibit intracellular accumulation of copper in the liver, suggesting a role in hepatic copper homeostasis (21). To test whether SLC46A3 recognizes copper ions, we performed an inhibition experiment using cupric chloride; however, no significant inhibition was observed.

We also measured intracellular copper levels in MDCKII/SLC46A3 dC and mock cells in the presence or absence of extracellular cupric chloride (40 μ M) and found no significant differences (Figure S6, Supplementary Material).

To compare the inhibitory potencies of steroid conjugates and bile acids on SLC46A3 dC, we evaluated the concentration-dependent transport of dehydroepiandrosterone sulfate, 25-hydroxyvitamin D₃ sulfate, pregnenolone sulfate, cholate, glycocholate, and taurocholate as substrates. All of these compounds significantly accumulated in MDCKII/SLC46A3 dC cells compared with mock cells (Figure S7, Supplementary Material). The uptake of dehydroepiandrosterone sulfate, 25-hydroxyvitamin D₃ sulfate, and pregnenolone sulfate were saturable with K_m values of 5.6 μ M, 0.2 μ M, and 1.2 μ M, respectively (Table 1), which were lower compared with that of estrone 3-sulfate. The uptake clearance (V_{max}/K_m) was the highest for 25-hydroxyvitamin D₃ sulfate, suggesting that it is the preferred substrate of SLC46A3 among those identified in this study. As the predicted LogD values at pH 5.0 for each compound followed the order, from highest to lowest, of 25-hydroxyvitamin D₃ sulfate, cholate, estrone 3-sulfate, pregnenolone sulfate, dehydroepiandrosterone sulfate, glycocholate, and taurocholate, uptake clearance was almost correlated with substrate lipophilicity, except for estrone 3-sulfate and cholate (Table 1). Therefore, the results suggest that SLC46A3 preferentially recognizes lipophilic steroid conjugates or bile acids as

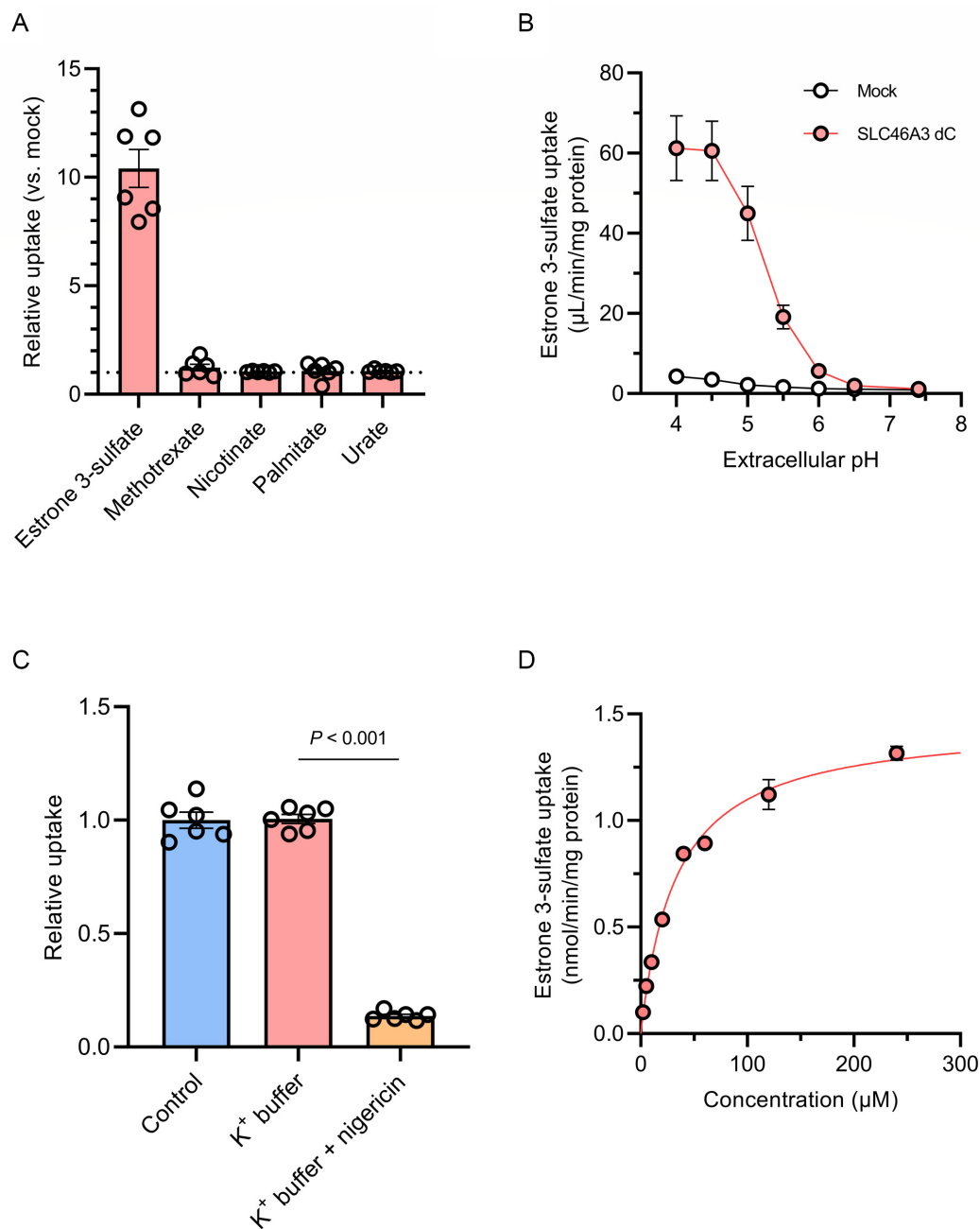


Fig. 2. SLC46A3 mediates proton-coupled estrone 3-sulfate uptake. (A) Uptake of [3 H]estrone 3-sulfate (10 nM), methotrexate (10 μ M), [3 H]nicotinate (200 nM), [3 H]palmitate (20 nM), and [14 C]urate (1.8 μ M) with 50 μ M urate in MDCKII/SLC46A3 dC cells. Uptake for 5 min was measured in HBSS (pH 5.5). Relative uptake was calculated by dividing the uptake in MDCKII/SLC46A3 dC cells by that in mock cells. (B) pH dependence of [3 H]estrone 3-sulfate (10 nM) uptake. Uptake for 1 min was measured in HBSS (pH 7.4) or modified-HBSS-containing citrate for pH 4.0 to 4.5, or MES for pH 5.0 to 6.5. (C) Effect of a proton gradient on [3 H]estrone 3-sulfate uptake. The uptake was measured in HBSS (pH 5.0) or modified-HBSS in which NaCl was replaced with KCl with or without 10 μ g/mL nigericin. (D) Concentration-dependent estrone 3-sulfate uptake. Uptake for 1 min was measured in HBSS (pH 5.0). SLC46A3 dC-specific uptake was calculated by subtracting the uptake in mock cells from that in MDCKII/SLC46A3 dC cells. The solid line represents the computer-fitted profile. Data are represented as the mean \pm SEM obtained from two biologically independent experiments. *P*-values are indicated in the different panels (one-way ANOVA followed by Tukey's multiple comparisons test).

endogenous substrates and may mediate escape from lysosomes to the cytoplasm *in vivo*.

SLC46A3 transports Lys-SMCC-DM1, mediating the cytotoxic effects of T-DM1

SLC46A3 downregulation in cancer cells results in T-DM1 resistance (5, 11, 13, 14). To examine whether SLC46A3 directly transports Lys-SMCC-DM1 (predicted $\text{LogD}_{5.0}$: 1.21), a major catabolite

of T-DM1 in lysosomes, uptake experiments were conducted using Lys-SMCC-DM1 in MDCKII/SLC46A3 dC cells. Lys-SMCC-DM1 was significantly accumulated in these cells compared with mock cells (Fig. 4A). DM1 (predicted $\text{LogD}_{5.0}$: 3.70), a payload of T-DM1, was also transported by SLC46A3, although it probably accumulated in mock cells by passive diffusion, suggesting that SLC46A3 recognizes the chemical structure of DM1. These uptakes were pH-sensitive (Fig. 4B), consistent with the pH dependency of estrone

Table 1. Kinetic parameters of SLC46A3 dC-mediated steroid conjugates uptake, and predicted LogP and LogD values of steroid conjugates and bile acids.

Compounds	K_m (μM)	V_{max} (nmol/min/mg protein)	LogP	LogD _{5.0}
Dehydroepiandrosterone sulfate	5.6 ± 1.1	1.51 ± 0.08	3.42	1.04
Estrone 3-sulfate	33.3 ± 2.7	1.46 ± 0.04	3.83	1.46
25-Hydroxyvitamin D ₃ sulfate	0.2 ± 0.1	0.27 ± 0.02	4.30	3.33
Pregnenolone sulfate	1.2 ± 0.4	0.79 ± 0.07	3.64	1.26
Cholate	26.7 ± 3.3	2.32 ± 0.09	2.48	1.84
Glycocholate	14.6 ± 2.7	1.31 ± 0.07	1.38	0.12
Taurocholate	11.7 ± 2.3	0.78 ± 0.04	-0.24	-1.46

The experiments were performed with two biological replicates to calculate the mean value of K_m and V_{max} for each compound. Data are presented as the mean ± SEM. ($n = 4$). Predicted LogP and LogD_{5.0} values of each compound were calculated with the online platform Chemicalize developed by ChemAxon (<http://chemicalize.com>).

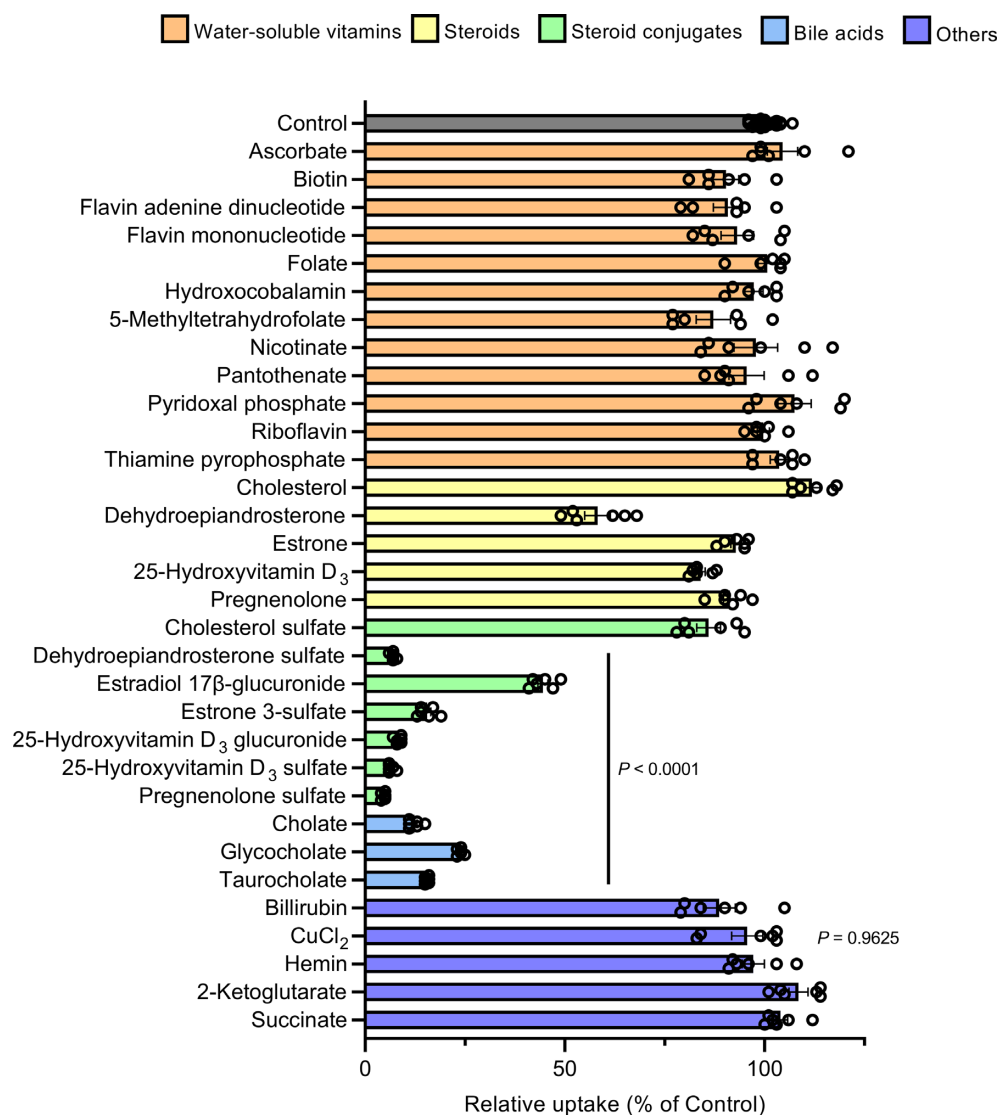


Fig. 3. Steroid conjugates and bile acids strongly suppress SLC46A3 dC-mediated estrone 3-sulfate transport. Effect of various compounds on the uptake of [³H]estrone 3-sulfate (10 nM) in MDCKII/SLC46A3 dC cells. Uptake was performed at 37°C, pH 5.0, for 1 min in the absence or presence of inhibitors (20 μM for cholesterol, dehydroepiandrosterone, estrone, pregnenolone, 25-hydroxyvitamin D₃, 25-hydroxyvitamin D₃ glucuronide, 25-hydroxyvitamin D₃ sulfate, hemin, and bilirubin or 200 μM for the other compounds). Data are presented as the mean ± SEM from two biologically independent experiments. P-values are indicated in the different panels (one-way ANOVA followed by Dunnett's multiple comparison).

3-sulfate uptake by SLC46A3 dC (Fig. 2B). Furthermore, the uptake of estrone 3-sulfate in MDCKII/SLC46A3 dC cells was significantly inhibited by Lys-SMCC-DM1 and DM1 (Fig. 4C). Conversely, the uptake of Lys-SMCC-DM1 and DM1 was significantly inhibited by

estrone 3-sulfate (Fig. 4D), indicating that Lys-SMCC-DM1 and DM1 were directly recognized and transported by SLC46A3.

These results indicate that any compound significantly inhibiting SLC46A3 transport function could reduce T-DM1 efficacy

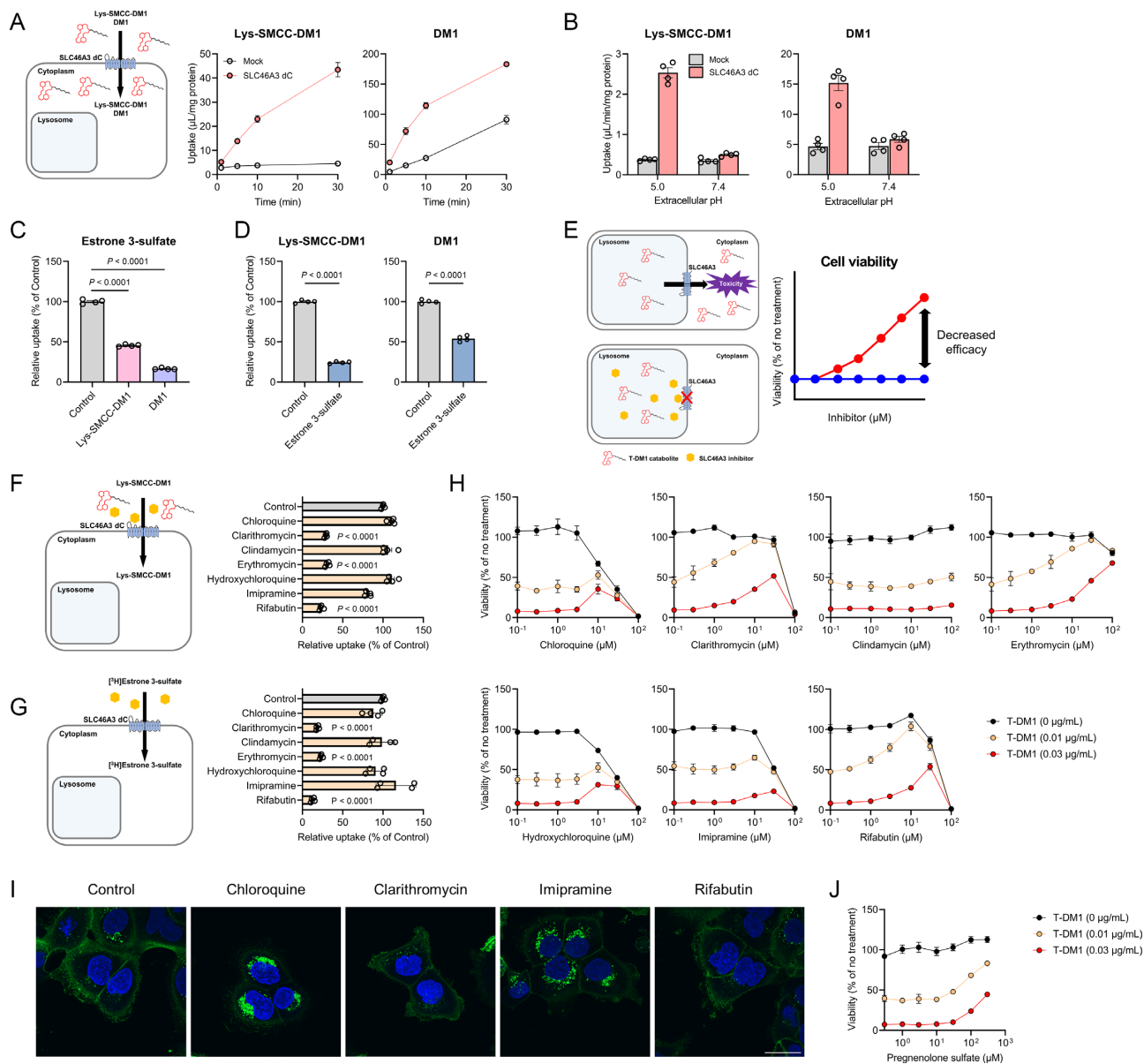


Fig. 4. SLC46A3 mediates T-DM1 cytotoxicity by directly transporting Lys-SMCC-DM1. (A) Time-dependent uptake of Lys-SMCC-DM1 (5 μM) and DM1 (1 μM) in the MDCKII/SLC46A3 dC cells. Uptake was performed at pH 5.0. Data are represented as the mean \pm SEM obtained from two biologically independent experiments. (B) pH-dependent uptake of Lys-SMCC-DM1 (5 μM) and DM1 (1 μM) in the MDCKII/SLC46A3 dC cells. Data are represented as the mean \pm SEM obtained from two biologically independent experiments. (C) Inhibitory effect of Lys-SMCC-DM1 and DM1 on the uptake of ^3H estrone 3-sulfate (10 nM) in MDCKII/SLC46A3 dC cells. Uptake was performed at pH 5.0 in the absence or presence of Lys-SMCC-DM1 and DM1 (200 μM). Data are represented as the mean \pm SEM obtained from two biologically independent experiments. P -values are indicated in the different panels (one-way ANOVA followed by Dunnett's multiple comparison). (D) Inhibitory effect of estrone 3-sulfate on the uptake of Lys-SMCC-DM1 (10 μM) and DM1 (1 μM). Uptake was performed at pH 5.0 in the absence or presence of estrone 3-sulfate (200 μM). Data are presented as the mean \pm SEM from two biologically independent experiments. P -values are indicated in the different panels (two-tailed unpaired t test). (E) Predicted schematic and results of Lys-SMCC-DM1–drug interaction through SLC46A3 in lysosomes. Impairment of lysosomal SLC46A3 function by a potent SLC46A3 inhibitor cause the inhibition of Lys-SMCC-DM1 escape from lysosomes, thereby reducing T-DM1 cytotoxicity. The predicted profiles of cell viability treated with T-DM1 in the presence (a red line) or absence (a blue line) of a SLC46A3 inhibitor are shown. (F) and (G) Inhibitory effect of lysosomotropic drugs on the uptake of Lys-SMCC-DM1 (5 μM) (F) or ^3H estrone 3-sulfate (10 nM) (G) in MDCKII/SLC46A3 dC cells. Uptake was performed at pH 5.0 in the absence or presence of lysosomotropic drugs (200 μM). Data are represented as the mean \pm SEM obtained from two biologically independent experiments. P -values are indicated in the different panels (one-way ANOVA followed by Dunnett's multiple comparison). (H) Effect of lysosomotropic drugs on T-DM1 cytotoxicity. SK-BR-3 cells were exposed to T-DM1 (0 $\mu\text{g}/\text{mL}$; black, 0.01 $\mu\text{g}/\text{mL}$; yellow, and 0.03 $\mu\text{g}/\text{mL}$; red) for 4 days in the presence of lysosomotropic drugs as indicated. Data are represented as the mean \pm SEM obtained from two biologically independent experiments. (I) Immunofluorescence staining of T-DM1 (green). HCC1954 cells were pulsed with 1.5 $\mu\text{g}/\text{mL}$ T-DM1 for 15 min at 37°C, and chased for 1 day in the presence or absence of chloroquine (10 μM), clarithromycin (30 μM), imipramine (30 μM), and rifabutin (30 μM). The results were replicated in two biologically independent experiments. Blue color, nucleus. Scale bar, 30 μm . (J) Effect of pregnenolone sulfate on T-DM1 cytotoxicity. SK-BR-3 cells were exposed to T-DM1 (0 $\mu\text{g}/\text{mL}$; black, 0.01 $\mu\text{g}/\text{mL}$; yellow, and 0.03 $\mu\text{g}/\text{mL}$; red) for 4 days with pregnenolone sulfate as indicated concentration. Data are presented as the mean \pm SEM obtained from two biologically independent experiments.

(Fig. 4E). Considering the lysosomal lumen as a potential binding site for Lys-SMCC-DM1 and other inhibitors, we selected drugs that tend to accumulate in lysosomes (i.e. lysosomotropic drugs) (22–24) and evaluated their inhibitory effects on Lys-SMCC-DM1 uptake in MDCKII/SLC46A3 dC cells. The SLC46A3-mediated Lys-SMCC-DM1 uptake was significantly inhibited by clarithromycin, erythromycin, and rifabutin, whereas other compounds such as chloroquine, clindamycin, and imipramine could not inhibit the uptake (Fig. 4F). Similarly, these lysosomotropic drugs also inhibited SLC46A3-mediated estrone 3-sulfate uptake (Fig. 4G).

We also determined whether some of these lysosomotropic drugs are transported by SLC46A3 in a proton-dependent manner (Figure S8, Supplementary Material). The uptakes of clarithromycin and rifabutin at pH 5.0 in MDCKII/SLC46A3 dC cells were comparable to those in mock cells. The erythromycin uptake was modestly increased in MDCKII/SLC46A3 dC cells, but the uptake activity of erythromycin was much lower than that of bile acid and steroid conjugates (Figure S7, Supplementary Material). These data indicate that lysosomotropic drugs that inhibit SLC46A3 function are simply blockers rather than substrates for SLC46A3. Furthermore, structure-based charge status prediction with Chemicalize (<https://chemicalize.com>) showed that clarithromycin, erythromycin, and rifabutin have a single positive charge at pH 5.0; Lys-SMCC-DM1 and DM1 are uncharged; and estrone 3-sulfate has a single negative charge (Table S1, Supplementary Material). Collectively, these results indicate that SLC46A3 is unlikely to recognize positively charged compounds as preferable substrates.

To evaluate whether SLC46A3 inhibitors affect the efficacy of T-DM1, we assessed the viability of SK-BR-3 cells, a breast cancer cell line overexpressing HER2, which were exposed to T-DM1 for 4 days in the presence of lysosomotropic drugs. The concentrations of T-DM1 used in this study were selected based on the LD₅₀ value against SK-BR-3 cells (Figure S9, Supplementary Material). As expected, potent SLC46A3 inhibitors, such as clarithromycin, erythromycin, and rifabutin, significantly reversed the cell viability from approximately 50% to 100% in the presence of 0.01 $\mu\text{g}/\text{mL}$ T-DM1 and approximately 10% to 50% in the presence of 0.03 $\mu\text{g}/\text{mL}$ T-DM1 (Fig. 4H), indicating the attenuation of T-DM1 cytotoxicity by these drugs. In contrast, other lysosomotropic drugs that little inhibited SLC46A3, such as chloroquine, hydroxychloroquine, and imipramine, demonstrated only a modest recovery of cell viability, and clindamycin demonstrated no significant effect on T-DM1 cytotoxicity in the evaluated concentration range. Similar results were obtained in HCC1954 and KPL-4 cells that are HER2-positive breast cancer cell lines, except for prominently recovered cell viability in the presence of chloroquine, hydroxychloroquine, and imipramine (Figure S10, Supplementary Material). The effects of chloroquine, hydroxychloroquine, and imipramine on T-DM1 cytotoxicity differed from cell to cell due to differences in the adaptation mechanism for lysosomal stress (25, 26); however, the reason is not clear.

To determine the inhibitory effect of the attenuation of T-DM1 efficacy by lysosomotropic drugs on the lysosomal degradation of T-DM1, we performed immunofluorescence analysis using an Alexa Fluor 488-conjugated antihuman IgG antibody that enables visualization of nondegraded IgG after T-DM1 internalization in the cells (27). HCC1954 cells were incubated with T-DM1 in the presence or absence of chloroquine, clarithromycin, imipramine, and rifabutin for 15 min. Intense T-DM1 staining was observed in cells treated with chloroquine and imipramine (Fig. 4I), suggesting that chloroquine and imipramine inhibited T-DM1 degradation in subcellular compartments, thereby reducing T-DM1

efficacy. These results of chloroquine and imipramine were consistent with previous studies (27). In contrast, T-DM1 staining in cells treated with clarithromycin and rifabutin was similar to that of the control (Fig. 4I), indicating that lysosomal T-DM1 degradation was not affected by clarithromycin and rifabutin.

Pregnenolone sulfate, which was identified to be a high affinity SLC46A3 substrate (Table 1) and is unlikely to be lysosomotropic, also reversed the cell viability in the higher concentration range (Fig. 4J). As pregnenolone sulfate has low membrane permeability and requires a transporter to permeate across the plasma membrane (Figure S7, Supplementary Material), it can be assumed that the intracellular level of pregnenolone sulfate is lower than its extracellular level. Moreover, the concentration might be much lower in lysosomes. Therefore, in contrast to lysosomotropic drugs, a relatively high extracellular concentration of pregnenolone sulfate could be required to inhibit the function of SLC46A3 in lysosomes.

Based on the above, it was suggested that SLC46A3 inhibitors reduce T-DM1 efficacy by inhibiting the escape of Lys-SMCC-DM1 from lysosomes into the cytoplasm.

Discussion

To date, although it was reported that SLC46A3 is essential for the potency of some noncleavable linker ADCs, its biochemical function and role in ADCs therapies have remained undefined. In the present study, we discovered that SLC46A3 is a proton-coupled, lysosomal steroid conjugate and bile acid transporter, by providing a detailed characterization of the transport activity. Furthermore, we found that SLC46A3 directly transports Lys-SMCC-DM1 and that potent SLC46A3 inhibitors caused the attenuation of T-DM1 potency. Our findings reveal the key role of SLC46A3 in T-DM1 efficacy at the molecular level, providing insights into the drug development of noncleavable ADCs.

The functional feature of SLC46A3 as a proton-dependent steroid conjugate transporter is quite unique among the SLC family members in mammals. Although there are many transporters capable of transporting steroid conjugates, including members of the SLC10A, SLC17A, SLC22A, and OATP/SLCO families, these are driven by a sodium gradient, membrane potential, exchange mechanisms with organic anions, and with bicarbonate, respectively (28–31). Notably, all transporters primarily localize at the plasma membrane and are involved in the transport of steroid conjugates across the plasma membrane. In contrast, SLC46A3 is localized to the lysosomes (Fig. 1B), which is consistent with previous reports (10, 21), and is likely driven by an outwardly directed proton gradient across the lysosomal membrane. This idea is supported by our findings that SLC46A3 transport activity requires a proton gradient and is optimal at the pH corresponding to that of lysosomes. Steroid conjugates are delivered to lysosomes by endocytic pathway via transport proteins such as albumin, vitamin D binding protein, and lipoproteins (32–34). Therefore, SLC46A3 may be involved in the lysosomal escape of steroid conjugates.

Our findings demonstrated that SLC46A3 transports Lys-SMCC-DM1, a major catabolite of T-DM1 in lysosomes (Fig. 4A), and is inhibited by several lysosomotropic drugs, which confirmed the mechanism of SLC46A3 in T-DM1 efficacy. Hamblett et al. (11) proposed a role of SLC46A3 as a lysosomal Lys-SMCC-DM1 exporter, by demonstrating that SLC46A3 knockdown caused T-DM1 resistance and entrapment of Lys-SMCC-DM1 in lysosomes. Taken together, the internalized T-DM1, after binding to HER2 is degraded in lysosomes to release Lys-SMCC-DM1, is transported by SLC46A3

across the lysosomal membrane into the cytoplasm, resulting in cytotoxicity by tubulin inhibition. This suggested pathway is further supported by our findings showing that effective SLC46A3 inhibitors, such as clarithromycin, erythromycin, and rifabutin, significantly reduce T-DM1 cytotoxicity, which is consistent with the fact that the downregulation of SLC46A3 expression in cancer cells is associated with T-DM1 resistance (13, 14). The lysosomotropic drugs accumulate significantly in acidic compartments, such as endosomes and lysosomes, based on an ion-trapping mechanism (23, 24). Thus, it is convinced that lysosomotropic SLC46A3 inhibitors reduce T-DM1 cytotoxicity by inhibition of SLC46A3 activity to escape Lys-SMCC-DM1 across the lysosomal membrane.

Notably, SLC46A3 mediates the lysosome-to-cytoplasm-directed transport with broad substrate specificity and can transport a relatively large molecule like Lys-SMCC-DM1. In this study, we demonstrated that SLC46A3 transports various steroids conjugated with sulfate and glucuronide as well as Lys-SMCC-DM1 and DM1 that are structurally unrelated to steroid conjugates (Fig. 4A; Figure S7, Supplementary Material). Specifically, SLC46A3 transported Lys-SMCC-DM1 owing to its relatively high molecular weight (MW: 1103.7). Thus, the substrate specificity of SLC46A3 is probably broader than that of other lysosomal transporters (35–39). Although ABCB1/MDR1/P-gp is a multidrug transporter that is localized not only in the plasma membrane but also partially in lysosomes, lysosomal ABCB1 mediates its substrate transport directed from the cytoplasm to lysosomes, indicating the significance of lysosomal sequestration of xenobiotics as a drug elimination pathway (40). In contrast, it could be suggested that SLC46A3 plays an essential role in the lysosomal egress of xenobiotics through endocytosis. Further studies on the substrate recognition of SLC46A3 are required to examine SLC46A3 function in drug delivery.

SLC46A3 is likely to be targeted to lysosomes by a tyrosine-based lysosomal sorting motif in its C-terminal region. We demonstrated that SLC46A3 mainly localizes to lysosomes and deletion of the C-terminal region (Y446–C463) causes SLC46A3 to localize to the plasma membrane, which is supported by the results of the direct transport assay using SLC46A3 dC (Fig. 2). These results indicate that the lysosomal localization of SLC46A3 is mainly regulated by its C-terminal region (Y446–C463). Indeed, the Y446A/L449A mutant SLC46A3 (SLC46A3 [AELA]) in HEK293T cells also localized to the plasma membrane, similar to SLC46A3 dC (Figure S11, Supplementary Material). Thus, the sequence of Y446–L449, which is shared among some mammalian species, is probably a tyrosine-based lysosomal sorting motif.

The results of this study are important for considering the clinical drug–drug interactions (DDIs) of T-DM1. Of the lysosomotropic agents that modulate T-DM1 cytotoxicity, clarithromycin exhibited potent inhibition at clinically relevant concentrations (1 to 4 μ M) (41), although the concentrations needed to significantly inhibit SLC46A3 function are much higher (Fig. 4F–H). Since lysosomotropic drugs extensively accumulate in acidic compartments, such as endosomes and lysosomes owing to an ion-trapping mechanism (23, 24), their inhibitory potency may be altered by the lysosomal pH, sequestration mechanism, and extracellular concentration. Therefore, T-DM1–SLC46A3 inhibitor interactions may be clinically relevant as potential DDIs during T-DM1 therapy. Further studies regarding T-DM1–drug interactions through SLC46A3 *in vivo* are needed.

The physiological role of SLC46A3 remains relatively unclear despite identification of its endogenous substrates. A recent study using *Slc46a3* KO mice (21) revealed that SLC46A3 is implicated

in hepatic copper homeostasis and lipid metabolism. However, in the present study, no endogenous substrates associated with copper metabolism could be identified. Our results clearly demonstrate that SLC46A3 facilitated the uptake of steroid conjugates and bile acids, whereas estrone sulfate uptake was not affected by cupric chloride. Thus, SLC46A3 might indirectly impact intracellular copper dynamics by regulating signaling of deconjugated steroids or bile acids although a specific associated mechanism remains unknown. Further studies are required to elucidate the role of SLC46A3 in copper homeostasis.

In conclusion, we have clarified the function of the orphan transporter, SLC46A3, as a novel proton-coupled steroid conjugate and bile acid transporter. We also discovered the SLC46A3 function as a Lys-SMCC-DM1 transporter and a T-DM1–drug interaction through SLC46A3. Our findings provide clues for understanding the role of SLC46A3 in the body and for proper use and development of pharmaceutical agents that target SLC46A3.

Methods

Reagents

[³H]Estrone 3-sulfate and [³H]palmitic acid were obtained from Perkin-Elmer, Inc. (Waltham, MA, USA). [³H]Nicotinic acid and [¹⁴C]uric acid were purchased from American Radiolabeled Chemicals Inc. (St. Louis, MO, USA). Estrone 3-sulfate sodium salt and 5-methyltetrahydrofolic acid disodium salt were procured from Sigma-Aldrich Co. Ltd. (St. Louis, MO, USA). L-Ascorbic acid, bilirubin, cholesterol, cholic acid (CA), copper (II) chloride, erythromycin, estrone, folic acid, hydroxocobalamin acetate, nicotinic acid, nigericin sodium salt, pyridoxal phosphate, sodium taurocholate (TCA), and succinic anhydride were obtained from FUJIFILM Wako Pure Chemical Industries, Ltd. (Osaka, Japan). Chloroquine diphosphate, clarithromycin, dehydroepiandrosterone, flavin adenine dinucleotide disodium salt hydrate, riboflavin 5'-monophosphate sodium salt, hemin, hydroxychloroquine sulfate, imipramine hydrochloride, methotrexate hydrate, pregnenolone, and uric acid were obtained from Tokyo Chemical Industry Co., Ltd. (Tokyo, Japan). Ansamitocin P-3, cholesterol sulfate sodium salt, dehydroepiandrosterone sulfate sodium salt (DHEAS), estradiol 17- β -D-glucuronide sodium salt hydrate, 25-hydroxyvitamin D₃, mertansine (DM1), pregnenolone sulfate sodium salt, and rifabutin were procured from Cayman Chemical Company (Ann Arbor, MI, USA). D-Biotin, 2-ketoglutaric acid, D-pantothenic acid sodium salt, riboflavin, and thiamine pyrophosphate chloride were purchased from Nacalai Tesque, Inc. (Kyoto, Japan). 25-Hydroxyvitamin D₃ glucuronide and 25-hydroxyvitamin D₃ sulfate were purchased from Toronto Research Chemicals Inc. (Toronto, Canada). Clindamycin hydrochloride and glycocholic acid sodium salt (GCA) were purchased from BLD Pharmatech Ltd. (Shanghai, China). Lys-SMCC-DM1 trifluoroacetate was procured from InvivoChem (Libertyville, IL, USA). KADCYLA (trastuzumab emtansine) was obtained from CHUGAI PHARMACEUTICAL CO., LTD. (Tokyo, Japan). All other chemicals were of analytical grade. Anti-FLAG antibody (Cat# F3165, RRID: AB_259529) was purchased from Sigma-Aldrich Co. Ltd. Antimouse IgG H&L Alexa fluor 488 (Cat# ab150113, RRID: AB_2576208) was obtained from Abcam (Cambridge, United Kingdom). Alexa Fluor 488-conjugated Antihuman IgG (H + L) (Cat# 109-545-003, RRID: AB_2337831) was purchased from Jackson Immuno Research Laboratories (West Grove, PA, USA). Cell Counting kit-8 was purchased from Dojindo Laboratories (Kumamoto, Japan). KOD plus mutagenesis kit was obtained from Toyobo Co.,

Ltd. (Osaka, Japan). NEBuilder HiFi DNA Assembly Master Mix was procured from New England Biolabs (Ipswich, MA, USA).

Cell culture

HEK293T, MDCKII, and KPL-4 (42) cells were maintained in Dulbecco's modified Eagle's medium (DMEM). SK-BR-3 (JCRB Cell Bank) and HCC1954 cells (JCRB Cell Bank) were cultured in RPMI 1640 medium. All media were supplemented with 10% fetal bovine serum, 100 units/mL penicillin G and 100 μ g/mL streptomycin. The cells were maintained at 37°C and 5% CO₂.

Generation and mutagenesis of SLC46A3-expressing plasmids

The coding region for human SLC46A3 was amplified using the EcoRI-containing forward primer 5'-GG GGGAATTCGCCG CCATGAAGATTTTATTGTAGAAC-3', and the Xba I-containing reverse primer 5'-CCCCTCTAGATTAACAGGCTCTGTCTGAA GCATC-3'. The PCR product was digested with restriction enzymes and subcloned into the pCI-neo vector (Promega, WI, USA). 3 × FLAG-C-pCI-neo vector was generated by insertion of the 3 × FLAG cDNA, which amplified from pmNeonGreenHO-3 × FLAG-G (RRID: Addgene_127914), into 3' region of multi cloning site in the pCI-neo vector. The human SLC46A3 cDNA was replaced into 3 × FLAG-C-pCI-neo vector, generating the SLC46A3-3 × FLAG-expression plasmid (SLC46A3-3 × FLAG/pCI-neo). According to the manufacturer's instructions, the SLC46A3-3 × FLAG/pCI-neo vector was modified using KOD plus mutagenesis kit, generating the SLC46A3 dC-3 × FLAG-expression plasmid. To construct hygromycin resistance (HygR)-T2A-SLC46A3 dC/pCI vector, 3 fragments of HygR-T2A, SLC46A3 dC and pCI were amplified using the following primers from pCW57-MCS1-P2A-MCS2 (RRID: Addgene_80922), FLAG-SLC46A3 dC/pCI-neo, and pCI vector, respectively; HygR-T2A: forward 5'-CTGACACAA CAGTCTCGAACTTAAGCTGCAGCCGCGATGAAAAAG CCTGA-3', reverse 5'-TGGACCAGGTTTCTTCAACATCACCACAAGTG-3', SLC46A3 dC: forward 5'-GTGGTGATGTTGAAGAAAACCTGGT CCAATGAAGATTTTATTGTAGAAC-3', reverse 5'-CAATGTATCTT ATCATGTCTGCTCGAAGCTCAGCTTCCCTCATTCAGCTGG-3', and pCI: forward 5'-GCTTCGAGCAGACATGATAAG-3', reverse 5'-CTGCAGCTTAAGTTCGAGAC -3'. These fragments were assembled using NEBuilder HiFi DNA Assembly Master Mix according to the manufacturer's protocol. Each construct was verified by sequencing.

Organelle marker protein-expressing plasmids

mCherry-Rab5a-7 (RRID: Addgene_55126) and mCh-Rab7A (RRID: Addgene_61804) were obtained from Addgene (Cambridge, MA, USA). cDNA of LAMP1 and calnexin were cloned into pmKate2-N vector (Evrogen, Moscow, Russia). cDNA of Peroxisomal targeting signal 1 (PTS1), N-terminal 81-amino acid human beta-1,4-galactosyltransferase [B4GALT (NT)], and mitochondrial targeting sequence (MTS) were amplified from pDsRed2-Peroxi vector, pAcGFP1-Golgi vector, and pAcGFP1-Mito vector (Takara Bio Inc., Shiga, Japan), respectively, and cloned into pmKate2-C vector (Evrogen).

Transfection

For preparing of HEK293T cells transiently expressing SLC46A3, HEK293T cells (1.5 × 10⁵ cells/well) were cultured on 24-well plates over 12 h, and then transfected with 1 μ g/well of plasmid by using 2 μ g/well of polyethylenimine (PEI) MAX (Mw 40,000; Polysciences, Inc., PA, USA). For immunofluorescence staining,

transfected cells were seeded on a 35 mm glass-bottom dishes and cultured for 2 days. To generate MDCKII cells stably expressing SLC46A3 dC, MDCKII cells were transfected with the HygR-T2A-SLC46A3 dC/pCI vector by using PEI MAX and selected by hygromycin (400 μ g/mL).

Immunofluorescence staining

Transfected cells with SLC46A3-3 × FLAG or SLC46A3 dC-3 × FLAG/pCI-neo and organelle marker protein-expressing plasmid were washed twice with phosphate-buffered saline (PBS), and then fixed with 4%-paraformaldehyde in PBS (Nacalai Tesque) for 15 min. After washing twice, cells were permeabilized using PBS containing 0.25% TritonX-100 for 5 min, washed twice with PBS, and blocked with 10% bovine serum albumin (BSA) in PBS at 37°C for 30 min. The cells were incubated with the anti-FLAG primary antibody (1:500) at 4°C for overnight. After washing twice with PBS containing 0.1% Tween 20 (PBS-T), the cells were stained using Alexa fluor 488-conjugate secondary antibody (1:1,000) at 37°C for 60 min. The cells were washed twice with PBS-T, then stained nuclei with Hoechst 33342, and visualized by using a confocal microscopy FV3000 (Olympus, Tokyo, Japan).

Uptake studies

MDCKII cells stably expressing SLC46A3 dC (1.0 × 10⁵ cells/well) were grown on 24-well plates for 2 days. The cells were preincubated with 500 μ L of Hank's balanced salt solution [HBSS; 137 mM NaCl, 5.33 mM KCl, 4.17 mM NaHCO₃, 0.441 mM KH₂PO₄, 0.338 mM Na₂HPO₄, 0.407 mM MgSO₄, 0.493 mM MgCl₂, 5.56 mM glucose, 1.26 mM CaCl₂, 10 mM citrate (pH 4.0–4.5), MES (pH 5.0–6.5), or HEPES (pH 7.4)] at 37°C for 3 min, and then incubated with 300 μ L of HBSS containing a test compound for indicated time. When necessary, HBSS was modified as indicated. Uptake was stopped by adding 1 mL ice-cold HBSS (pH 7.4) (containing 1.5% BSA for the uptake study using 25-hydroxyvitamin D₃ sulfate), and the cells were washed 2 times with 2 mL ice-cold HBSS. The uptake incubation buffer was collected for each concentration to determine the unbound concentration of 25-hydroxyvitamin D₃ sulfate. After the uptake, for [³H]-labeled substrates uptake, the cells were solubilized with 500 μ L of 0.3 N NaOH solution containing 0.1% TritonX-100, and the accumulated radioactivity was measured by liquid scintillation counting. For other substrates uptake, the cells were extracted with 300 μ L of 50% acetonitrile (for DM1 and Lys-SMCC-DM1) or 500 μ L of 50% methanol (for other compounds) containing corresponding internal standard for 30 min at room temperature. The supernatant was filtered with a 0.2- μ m filter and then quantified by LC-MS/MS. In parallel, cells cultured under the same conditions were lysed with 500 μ L of 0.3 N NaOH solution containing 0.1% TritonX-100, and protein concentration was determined by Pierce BCA protein assay kit (Thermo Fisher Scientific, MA, USA). The uptake amount was normalized to cellular protein content.

LC-MS/MS

LC-MS/MS analyses of the test compounds in the uptake experiments were conducted on a Xevo TQD triple quadrupole tandem mass spectrometer coupled with an ACQUITY UPLC H-Class system (Waters, Milford, MA, USA). Methotrexate in the cellular uptake assays was quantified with antipyrine as the internal standard. Chromatographic separation was achieved on a UNISON UK-C18 HT (3 × 30 mm, 3 μ m) column (Imtakt, Kyoto, Japan). The mobile phase consisted of 0.1% formic acid (A) and acetonitrile (B). The flow rate was 0.2 mL/min with following gradient

programming: (1) 0 to 0.7 min: hold at 0% B; (2) 0.7 to 1.5 min: linear gradient from 0% to 95% B; (3) 1.5 to 3.4 min: hold at 95% B; (4) 3.4 to 3.5 min: linear gradient from 95% to 0% B; and (5) 3.5 to 4.5 min: hold at 0% B. The electrospray ionization was operated in the positive mode. Methotrexate and antipyrine were detected by multiple reaction monitoring (MRM) at m/z 455.2 to 308 and m/z 189.1 to 131, respectively. DHEAS, pregnenolone sulfate, and 25-hydroxyvitamin D₃ sulfate in the cellular uptake assays were quantified with estrone 3-sulfate as the internal standard. Chromatographic separation was achieved on a ZORBAX Eclipse Plus C18 (2.1 × 50 mm, 5 μm) column (Agilent Technologies, CA, USA). The mobile phase consisted of 10 mM ammonium acetate (pH 4.5) (A) and methanol (B). The flow rate was 0.2 mL/min with following gradient programming: (1) 0 to 1 min: hold at 30% B; (2) 1 to 2 min: linear gradient from 30% to 95% B; (3) 2 to 5 min: hold at 95% B; (4) 5 to 5.1 min: linear gradient from 95% to 30% B; and (5) 5.1 to 6.5 min: hold at 30% B. The electrospray ionization was operated in the negative mode. MRM detected DHEAS, pregnenolone sulfate, 25-hydroxyvitamin D₃ sulfate, and estrone 3-sulfate at m/z 367.1 to 97, m/z 395.1 to 97, m/z 479.3 to 97, and m/z 349.1 to 269.3, respectively. CA, GCA, and TCA were quantified with estrone 3-sulfate as the internal standard in the cellular uptake assays. Chromatographic separation was achieved on a ZORBAX Eclipse Plus C18 (2.1 × 50 mm, 5 μm) column (Agilent Technologies). The mobile phase consisted of 10 mM ammonium acetate (pH 4.5) (A) and methanol (B). The flow rate was 0.2 mL/min with following gradient programming: (1) 0 to 0.5 min: hold at 10% B; (2) 0.5 to 1.5 min: linear gradient from 10% to 95% B; (3) 1.5 to 5 min: hold at 95% B; (4) 5 to 5.1 min: linear gradient from 95% to 10% B; and (5) 5.1 to 7 min: hold at 10% B. The electrospray ionization was operated in the negative mode. MRM detected CA, GCA, TCA, and estrone 3-sulfate at m/z 407.3 to 343.3, m/z 464.3 to 74, m/z 514.2 to 80, and m/z 349.1 to 269.3, respectively. DM1 and Lys-SMCC-DM1 in the cellular uptake assays was quantified with ansamitocin P-3 as the internal standard. Chromatographic separation was achieved on a InertSustain C18 (2.1 × 100 mm, 5 μm) column (GL Science Co., Ltd., Tokyo, Japan). The mobile phase consisted of 0.1% formic acid (A) and 0.1% formic acid in acetonitrile (B). The flow rate was 0.2 mL/min with following gradient programming: (1) 0 to 0.5 min: hold at 5% B; (2) 0.5 to 3 min: linear gradient from 5% to 95% B; (3) 3 to 6.5 min: hold at 95% B; (4) 6.5 to 6.6 min: linear gradient from 95% to 5% B; and (5) 6.6 to 8 min: hold at 5% B. The electrospray ionization was operated in the positive mode. MRM detected at m/z 738.5 to 547.5 for DM1, m/z 1103.2 to 485.2 for Lys-SMCC-DM1, and m/z 635.2 to 547.2 for ansamitocin P-3.

T-DM1 cytotoxicity assay

SK-BR-3, HCC1954, and KPL-4 cells were seeded into 96-well plates at a density of 3,000 cells/well. The next day, the cells were treated with T-DM1 (0, 0.01, and 0.03 μg/mL) in the presence of the test compounds. Then, 4 days later, cell viability was determined using Cell Counting kit-8 (Dojindo). Absorbance at 450 nm was measured with a Varioskan Flash 2.4 microplate reader (Thermo Fisher Scientific). Cell viability was calculated as a percentage of untreated cells.

T-DM1 immunostaining

HCC1954 cells (1.0 × 10⁵ cells/dish) were seeded on 35 mm glass-bottom dishes. The next day, the cells were pulsed with T-DM1 (1.5 μg/mL) for 15 min at 37°C, followed by two washes in PBS. After the pulse, the cells were cultured for 1 day in the presence or absence of chloroquine (10 μM), clarithromycin

(30 μM), imipramine (30 μM), and rifabutin (30 μM). The cells were processed as “Immunofluorescence staining” in material and method section. Alexa fluor 488-conjugate antihuman IgG antibody (1:1,000) was used as a secondary antibody. Fluorescence images were captured with confocal microscopy FV1000 (Olympus).

Statistical analysis

Data are presented as the mean ± SEM. Comparisons between multiple groups were performed by using one-way analysis of variance (ANOVA) followed by Dunnett's multiple comparisons or Tukey's multiple comparisons test. For all statistical analyses, $P < 0.05$ was considered statistically significant. Statistical analysis was performed with GraphPad Prism v9.2.0 (RRID: SCR_002798).

Acknowledgments

We thank Professor Junichi Kurebayashi (Kawasaki Medical School, Japan) for kindly providing KPL-4 cells.

Supplementary Material

Supplementary material is available at [PNAS Nexus](#) online.

Funding

This work was supported in part by a research grant from the Grants-in-Aid for Scientific Research (18K06760 to K.I., 20H00568 to T.T., and 21K06678 to K.I.).

Authors' Contributions

R.T., H.K., and K.I. designed the research; R.T., T.S., and N.S. performed the research; K.K. contributed new reagents/analytical tools; R.T., K.H., T.T., and Y.S. analyzed the data; and R.T. and K.I. wrote the paper. Materials and correspondence: correspondence should be addressed to K.I.

Data Availability

All study data are included in the article and/or supporting information.

References

1. Chau CH, Steeg PS, Figg WD. 2019. Antibody-drug conjugates for cancer. *Lancet*. 394:793–804.
2. Khongorzul P, Ling CJ, Khan FU, Ihsan AU, Zhang J. 2020. Antibody-drug conjugates: a comprehensive review. *Mol Cancer Res*. 18:3–19.
3. Tsao L-C, Force J, Hartman ZC. 2021. Mechanisms of therapeutic antitumor monoclonal antibodies. *Cancer Res*. 81:4641–4651.
4. Coats S, et al. 2019. Antibody-drug conjugates: future directions in clinical and translational strategies to improve the therapeutic index. *Clin Cancer Res*. 25:5441–5448.
5. Tsui CK, et al. 2019. CRISPR-Cas9 screens identify regulators of antibody-drug conjugate toxicity. *Nat Chem Biol*. 15:949–958.
6. Kovtun YV, et al. 2006. Antibody-drug conjugates designed to eradicate tumors with homogeneous and heterogeneous expression of the target antigen. *Cancer Res*. 66:3214–3221.
7. Ogitani Y, Hagihara K, Oitate M, Naito H, Agatsuma T. 2016. Bystander killing effect of DS-8201a, a novel anti-human epidermal growth factor receptor 2 antibody-drug conjugate, in

- tumors with human epidermal growth factor receptor 2 heterogeneity. *Cancer Sci.* 107:1039–1046.
8. Pegram MD, Miles D, Tsui CK, Zong Y. 2020. HER2-overexpressing/amplified breast cancer as a testing ground for antibody-drug conjugate drug development in solid tumors. *Clin Cancer Res.* 26:775–786.
 9. Lewis Phillips GD, et al. 2008. Targeting HER2-positive breast cancer with trastuzumab-DM1, an antibody-cytotoxic drug conjugate. *Cancer Res.* 68:9280–9290.
 10. Chapel A, et al. 2013. An extended proteome map of the lysosomal membrane reveals novel potential transporters. *Mol Cell Proteomics.* 12:1572–1588.
 11. Hamblett KJ, et al. 2015. SLC46A3 is required to transport catabolites of noncleavable antibody maytansine conjugates from the lysosome to the cytoplasm. *Cancer Res.* 75:5329–5340.
 12. García-Alonso S, Ocaña A, Pandiella A. 2018. Resistance to antibody-drug conjugates. *Cancer Res.* 78:2159–2165.
 13. Kinneer K, et al. 2018. SLC46A3 as a potential predictive biomarker for antibody-drug conjugates bearing noncleavable linked maytansinoid and pyrrolbenzodiazepine warheads. *Clin Cancer Res.* 24:6570–6582.
 14. Li G, et al. 2018. Mechanisms of acquired resistance to trastuzumab emtansine in breast cancer cells. *Mol Cancer Ther.* 17:1441–1453.
 15. Zhao R, Goldman ID. 2013. Folate and thiamine transporters mediated by facilitative carriers (SLC19A1-3 and SLC46A1) and folate receptors. *Mol Aspects Med.* 34:373–385.
 16. Bonifacino JS, Traub LM. 2003. Signals for sorting of transmembrane proteins to endosomes and lysosomes. *Annu Rev Biochem.* 72:395–447.
 17. Department of Health and Human Services. 2020. In vitro drug interaction studies - cytochrome P450 enzyme and transporter mediated drug interactions guidance for industry. Rockville (MD): US Food and Drug Administration Center for Drug Evaluation and Research (CDER).
 18. Qiu A, et al. 2006. Identification of an intestinal folate transporter and the molecular basis for hereditary folate malabsorption. *Cell.* 127:917–928.
 19. Nakai Y, et al. 2007. Functional characterization of human proton-coupled folate transporter/heme carrier protein 1 heterologously expressed in mammalian cells as a folate transporter. *J Pharmacol Exp Ther.* 322:469–476.
 20. Mindell JA. 2012. Lysosomal acidification mechanisms. *Annu Rev Physiol.* 74:69–86.
 21. Kim J-H, et al. 2021. Lysosomal SLC46A3 modulates hepatic cytosolic copper homeostasis. *Nat Commun.* 12:290.
 22. Norinder U, Tuck A, Norgren K, Munic Kos V. 2020. Existing highly accumulating lysosomotropic drugs with potential for repurposing to target COVID-19. *Biomed Pharmacother.* 130:110582.
 23. Schmitt MV, Lienau P, Fricker G, Reichel A. 2019. Quantitation of lysosomal trapping of basic lipophilic compounds using in vitro assays and in silico predictions based on the determination of the full pH profile of the endo-/lysosomal system in rat hepatocytes. *Drug Metab Dispos.* 47:49–57.
 24. de Duve C, et al. 1974. Commentary. Lysosomotropic agents. *Biochem Pharmacol.* 23:2495–2531.
 25. Collins KP, Witts S, Coy JW, Pang Y, Gustafson DL. 2021. Lysosomal biogenesis and implications for hydroxychloroquine disposition. *J Pharmacol Exp Ther.* 376:294–305.
 26. Nilsson C, Roberg K, Grafström RC, Ollinger K. 2010. Intrinsic differences in cisplatin sensitivity of head and neck cancer cell lines: correlation to lysosomal pH. *Head Neck.* 32:1185–1194.
 27. Ríos-Luci C, et al. 2017. Resistance to the antibody-drug conjugate T-DM1 is based in a reduction in lysosomal proteolytic activity. *Cancer Res.* 77:4639–4651.
 28. Jutabha P, et al. 2010. Human sodium phosphate transporter 4 (hNPT4/SLC17A3) as a common renal secretory pathway for drugs and urate. *J Biol Chem.* 285:35123–35132.
 29. Claro da Silva T, Polli JE, Swaan PW. 2013. The solute carrier family 10 (SLC10): beyond bile acid transport. *Mol Aspects Med.* 34:252–269.
 30. Leuthold S, et al. 2009. Mechanisms of pH-gradient driven transport mediated by organic anion polypeptide transporters. *Am J Physiol Cell Physiol.* 296:C570–C582.
 31. Sekine T, Miyazaki H, Endou H. 2006. Molecular physiology of renal organic anion transporters. *Am J Physiol Renal Physiol.* 290:F251–F261.
 32. Puche RC, Nes WR. 1962. Binding of dehydroepiandrosterone sulfate to serum albumin. *Endocrinology.* 70:857–863.
 33. Willnow TE, Nykjaer A. 2010. Cellular uptake of steroid carrier proteins—mechanisms and implications. *Mol Cell Endocrinol.* 316:93–102.
 34. Wong T, et al. 2018. Polymorphic human sulfotransferase 2A1 mediates the formation of 25-hydroxyvitamin D3-3-O-sulfate, a major circulating vitamin D metabolite in humans. *Drug Metab Dispos.* 46:367–379.
 35. Kalatzis V, Cherqui S, Antignac C, Gasnier B. 2001. Cystinosin, the protein defective in cystinosis, is a H(+)-driven lysosomal cystine transporter. *EMBO J.* 20:5940–5949.
 36. Morin P, Sagné C, Gasnier B. 2004. Functional characterization of wild-type and mutant human sialin. *EMBO J.* 23:4560–4570.
 37. Jézégou A, et al. 2012. Heptahelical protein PQLC2 is a lysosomal cationic amino acid exporter underlying the action of cysteamine in cystinosis therapy. *Proc Natl Acad Sci USA.* 109:E3434–E3443.
 38. Verdun Q, et al. 2017. SNAT7 is the primary lysosomal glutamine exporter required for extracellular protein-dependent growth of cancer cells. *Proc Natl Acad Sci USA.* 114:E3602–E3611.
 39. van Veen S, et al. 2020. ATP13A2 deficiency disrupts lysosomal polyamine export. *Nature.* 578:419–424.
 40. Yamagishi T, et al. 2013. P-glycoprotein mediates drug resistance via a novel mechanism involving lysosomal sequestration. *J Biol Chem.* 288:31761–31771.
 41. Rodvold KA. 1999. Clinical pharmacokinetics of clarithromycin. *Clin Pharmacokinet.* 37:385–398.
 42. Kurebayashi J, et al. 1999. Isolation and characterization of a new human breast cancer cell line, KPL-4, expressing the Erb B family receptors and interleukin-6. *Br J Cancer.* 79:707–717.